Effect of poly(ethylene glycol) on insulin stability and cutaneous cell proliferation *in vitro* following cytoplasmic delivery of insulin-loaded nanoparticulate carriers – a potential topical wound management approach

Dalia H. Abdelkader[1,2], Mohamed A. Osman[2], Sanaa A. El-Gizawy[2], Suzan J. Hawthorne[1], Ahmed M. Faheem[3] and Paul A. McCarron[1]*

[1]*School of Pharmacy and Pharmaceutical Sciences, Saad Centre for Pharmacy and Diabetes, Ulster University, Cromore Road, Coleraine, Co. Londonderry, BT52 1SA, UK.*

[2]*Faculty of Pharmacy, Pharmaceutical Technology Department, Tanta University, Tanta, 31111, Egypt.*

[3]*Sunderland Pharmacy School, University of Sunderland, Sunderland, SR1 3SD, UK.*

*Corresponding author
Prof. Paul A. McCarron
School of Pharmacy and Pharmaceutical Sciences,
University of Ulster,
Cromore Road,
Coleraine,
Co. Londonderry,
BT52 1SA, UK
Tel: +44 (0) 28 70123285
Fax: +44 (0) 28 70123518
Email: p.mccarron@ulster.ac.uk

Abstract

We describe the development of a nanoparticulate system, with variation of poly(ethylene glycol) (PEG) content, capable of releasing therapeutic levels of bioactive insulin for extended periods of time. Recombinant human insulin was encapsulated in poly(D,L-lactide-co-glycolide) nanoparticles, manufactured with variation in poly(ethylene glycol) content, and shown to be stable for 6 days using SDS-PAGE, western blot and MALDI MS. To determine if insulin released from this sustained release matrix could stimulate migration of cell types normally active in dermal repair, a model wound was simulated by scratching confluent cultures of human keratinocytes (HaCaT) and fibroblast (Hs27). An important finding of this work was that closure of the scratch fissures was significantly faster in the presence of nano-encapsulated insulin when compared to the free form, with a more pronounced effect observed in HaCaT cells when compared to Hs27 cells. Variation in PEG content had the greatest effect on NP size, with a lesser influence on scratch closure times. Our work supports a particulate uptake mechanism that provides for intracellular insulin delivery, leading to enhanced cell proliferation. When placed into an appropriate topical delivery vehicle, such as hydrogel, the extended and sustained topical administration of active insulin delivered from a nanoparticulate vehicle shows promise in promoting tissue healing.

Keywords

Sustained topical delivery; insulin-loaded PLGA NP; poly(ethylene glycol); wound scratch closure; keratinocyte; fibroblasts

1. Introduction

Insulin, a peptide hormone with multiple physiological roles, restores integrity of damaged skin. It is of interest in the field of wound repair, due particularly to low cost relative to other peptide-based growth factors. Its beneficial effects first became apparent after discernible differences were recorded in the rate of postoperative wound healing between diabetic and non-diabetic patients [1]. In the former group, wounds were less likely to re-epithelialise normally, making them susceptible to infection. Such findings prompted the development and evaluation of the therapeutic benefits of insulin when incorporated into wound dressings, bioadhesive films and hydrogels [1]. Recalcitrant, non-healing wounds remain a major healthcare challenge that plagues patients with chronic illness. Notwithstanding systemic insulin therapy and a carefully regulated life style, approximately 15% of all diabetic patients will have some form of non-healing wound and be susceptible to amputation of the lower extremities [2].

Direct administration of insulin to the wound surface is known to be clinically effective, especially when the rate of closure is considered. Results confirm that insulin stimulates keratinocyte migration in a dose and time dependent manner, acting in an insulin-receptor-dependent, but EGF/EGF-R-independent, manner [3]. Conversely, the ability to stimulate both the insulin and IGF-1 receptors may broaden the applicability of insulin in different wound types, particularly when one receptor may be dysfunctional (e.g. in Type II diabetes). Consequently, it has been shown that topically applied insulin increases wound tensile strength and accelerates healing in Wistar rats [4]. Similarly, topical administration to linear musculoperitoneal wounds in the murine model leads to faster wound healing, with histological examination demonstrating earlier appearance of collagen fibres with denser and well-oriented morphology [5]. Understanding the process by which insulin accelerates the wound closure is

important because it will provide insight into many potential applications directed to the healing process [6].

Several insulin-loaded formulation types have been developed and evaluated. For example, Lima *et al*. [7] investigated the effect of a topical cream, containing insulin, showing that it decreases wound healing time and induces a rescue in the levels of tissue proteins involved in the early steps of insulin action. Topical application of this patented insulin-containing cream was shown to normalise the wound healing time in diabetic animals. In a similar study, Achar *et al*. [8] showed that topical use of a cream containing insulin-like growth factor (IGF-1) improves wound healing in both diabetic and non-diabetic animals, with increased expression of fibroblasts. In addition, an insulin-containing, spray-based formulation has been used successfully to treat patients with diabetic ulcers [9]. These approaches, which deliver insulin in the free form, benefit from the location of the insulin receptor, which contains four sub-units and is located on the plasma membrane. This free insulin rapidly mediates the short-term effects on membrane function, such as the uptake of glucose, and the full biological effects are brought about when less than 10% of the total cell surface insulin receptors are occupied [10].

Recently, topical formulations have utilised nano-sized carriers as novel drug delivery vehicles, such as polymeric nanoparticles (NP), liposomes and nano-emulsions, to enhance cutaneous delivery of pharmaceutically active materials, such as topically applied peptides [11]. Colloidal vehicles sustain release, protect peptides and proteins from chemical and physical degradation, and provide targeting opportunities for cell-directed and tissue-specific targeting using conjugating techniques [12]. They are made from a wide range of polymeric materials, but poly(D,L-lactide-co-glycolide) (PLGA), being both biodegradable and biocompatible, has enjoyed widespread interest and is capable of controlled release for several days [13]. It can be

made in nanoparticulate form and loaded with a range of molecular drug substances and is amenable to the usual means of enhanced cutaneous delivery, such as iontophoresis [14]. Importantly, these nanoparticulate carriers can be endocytosed by cells and delivery of an encapsulated payload directly into the cytosol becomes feasible. Although insulin receptors reside on the plasma membrane, studies demonstrate their presence on intracellular organelles, such as the Golgi apparatus, endoplasmic reticulum and the nucleus [15]. As free insulin does not readily cross the plasma membrane, the use of endocytosed insulin-loaded carriers could provide a novel means to bring about binding to intracellular insulin receptors.

In this present study, we compared the effect of insulin on keratinocyte and fibroblast populations delivered by either intracellular nanoparticulate delivery or via the free form. The aim of the former approach was to investigate proliferative effects following activation of intracellular insulin receptors, whilst the latter approach would consider activation of membrane-bound receptors. Human recombinant insulin was loaded into PLGA NP using a modified, double-emulsion, solvent technique. Importantly, the effect of poly(ethylene glycol) content, which is known to affect both colloidal stability [16] and cellular uptake of colloidal carriers [17] was investigated. Nanoparticles were characterised according to encapsulation efficiency, surface morphology, particle size, polydispersity index (PDI), zeta potential and *in vitro* release profile. Insulin integrity and stability were assessed *in vitro* using SDS-PAGE, western blot and MALDI mass spectrometry. *In vitro* studies were performed on kerotinocyte and fibroblast cell lines in order to assess insulin-mediated cellular migration in the context of wound repair. A proposed mechanism of nanoparticulate uptake facilitated by endocytosis was investigated using inhibition of vesicle formation following exposure to dynasore hydrate.

2. Materials and Methods

2.1 Materials

Insulin, recombinant human, dry powder and poly(D,L-lactide-co-glycolide, acid terminated, lactide:glycolide 50:50, MW 24,000-38,000) were purchased from Sigma Aldrich, UK. Dimethylsulfoxide (DMSO), hydrochloric acid (HCl), acetic acid, trifluroacetic acid (TFA), trypan blue and crystal violet solutions were purchased from Fluka, Sigma Aldrich, UK. Poly(vinyl alcohol) (PVA, MW=31,000-50,000, 87-89% hydrolysed), poly(ethylene glycol) flakes (PEG, Mw 2000 Da and 5000 Da), sucrose powder and potassium chloride (KCl) were all purchased from Sigma Aldrich, UK. Dulbeco's phosphate-buffered saline (DPBS) and sodium hydroxide (NaOH) were purchased from Fisher Scientific, UK. A BCA Protein Assay Kit was purchased from Thermo Fisher Scientific, Pierce Biotechnology Inc., USA. 3-(4,5-Dimethylthiazol-2-yl)-2,5-diphenyl-tetrazolium bromide) was purchased from Arcos, Organics, New Jersey, USA.

Human keratinocytes (HaCaT) were provided by Cell Line Services, Eppelheim, Germany [18]. Human fibroblasts (Hs27) were supplied from ATCC, UK. Dulbecco's modified Eagle's medium (DMEM, 1X), fetal bovine serum (FBS), 0.5% trypsin-EDTA (10X) and penicillin streptomycin solution (Pen-Strep) were all purchased from Gibco® life technologies, UK. Dynasore hydrate was purchased from Sigma Aldrich, UK. Dichloromethane (DCM), trifluoroacetic acid (TFA), acetonitrile and methanol were of HPLC grade. All other reagents and solvents were of appropriate laboratory standard and used without further purification.

2.2 PLGA NP preparation

Insulin-loaded NP were prepared using a double-emulsion, solvent evaporation technique, adapted with minor modification [19]. Briefly, 0.1 ml of an aqueous insulin solution (5 mg, dissolved in a mixture of 0.1 M HCL and PVA 2.5 % w/v, pH 1-2) was added drop-wise to an organic phase (4.0 ml dichloromethane, DCM) comprising 100 mg of PLGA. This organic phase contained variations in PEG content, both in concentration and molecular weight, as defined by the Formula codes in Table 1. This primary emulsion was agitated in an ice bath for 120 s at 1000 rpm (Ultra-Turrax® T10 Basic Disperser, IKA® Works, VWR ®International, UK) before drop-wise addition to 50 ml of an external aqueous phase containing 1.25% w/v PVA [20], with continuous stirring in an ice bath for 360 s at 10,000 rpm (model L5M-A Silverson Ltd., UK). DCM was evaporated under magnetic stirring overnight. NP were collected by centrifugation (3-30k, Sigma Laboratory Centrifuge Henderson Biomedical Ltd., Germany) at 11,000 x *g* for 30 minutes at 4 ºC and washed with three sequential steps, 10 minutes for each, using distilled water, 2% w/v sucrose solution [21] then distilled water. The pellet was frozen at -20 ºC for 4-6 hours and then lyophilised (4.5 Plus, Labconco Ltd., USA) for 48 hours.

2.3 Particle size and zeta potential measurements

Surface charge (zeta potential, mV) was determined by measuring electrophoretic mobility. Particulate size (diameter, nm) and polydispersity index were determined by photon correlation spectrometry (ZetaSizer Nano series, Malvern Instruments, Worcestershire, UK), using a He-Ne laser operating at 633 nm and a fixed scattering angle of 90º. Measurements were performed in triplicate at 25 ºC for samples diluted in either distilled water or 1.0 mM KCl solution.

2.4 Chromatographic analysis

Aqueous concentrations of recombinant human insulin were determined using reversed phase HPLC (Shimadzu Corporation, Kyoto, Japan). Separation was performed on a Luna® C18 column (5 μm, 150×4.6 mm, Phenomenex, CA, USA). The mobile phase comprised a binary mixture of 0.1% trifluroacetic acid in water and 0.1% trifluroacetic acid in acetonitrile [22]. Gradient elution was applied by increasing acetonitrile concentration from 10% to 35% over a 15-minute period. Detection was at 210 nm with a flow rate of 1.1 ml per minute. Analysis was conducted at ambient temperature and peak area was used to quantify the analyte concentration.

2.5 Drug loading (DL) and entrapment efficiency (EE)

The amount of encapsulated insulin was determined by analysing protein content within the NP matrix (entrapped fraction), together with an analysis of the supernatant (non-entrapped protein fraction). The entrapped fraction was measured using a bicinchoninic acid assay following the digestion of lyophilised NP (15 mg) using 1.0 M NaOH for 2 hours and subsequent neutralisation with 1.0 M HCl [19]. Drug loading and direct EE (%) were calculated from Eq. (1) and (2), respectively [23].

$$\text{DL} = \frac{\text{Mass of drug in NP (mg)}}{\text{Mass of NP (mg)}} \quad (1)$$

$$\text{Direct EE (\%)} = \frac{\text{Mass of drug in NP (mg)}}{\text{Mass of drug used (mg)}} \times 100 \quad (2)$$

Insulin concentration in the supernatant was determined using RP-HPLC, as described in Section 2.4. This indirect EE (%) was calculated using Eq. (3) [24].

$$\text{Indirect \%EE} = \frac{\text{Total mass of drug used (mg)-mass of drug in supernatant (mg)}}{\text{Total mass of drug used (mg)}} \text{ x } 100 \qquad (3)$$

2.6 In vitro release kinetics

Lyophilised, insulin-loaded NP (15 mg) were suspended in 1.0 ml phosphate-buffered saline solution (PBS pH 7.4). The samples were placed in a rotating mixer (Stuart Rotator Drive STR4, Bibby Scientific Ltd., UK) at 100 rpm and incubated at 37 °C. Samples were withdrawn at predetermined time intervals over 6 days and centrifuged at 5500 x *g* (Mini-Spin Eppendorf, Davidson & Hardy Ltd., UK) for 5 minutes. The release medium was removed and 1.0 ml of fresh medium added [25]. Each sample was analysed using RP-HPLC, as described in Section 2.4.

2.7 Morphological characterisation

Lyophilised NP were vacuum-coated for 3 minutes with a mixture of gold and palladium and examined for morphology scanning electron microscopy at 20 kV (Zeiss, Oberkochen, Germany).

2.8 In vitro drug stability

Gel electrophoresis (SDS-PAGE) and western blotting

Samples (10 µl) of insulin standard, insulin released from NP and a protein ladder (See Blue® Plus2 Pre-stained Protein Standard, Novex ™ Thermo Fisher Scientific, UK) were applied to the wells of a NUPAGE® Bis-Tris 12 % gel (Invitrogen, Thermo Fisher Scientific, UK) using a mini-cell electrophoresis system (X-cell Surelock™, Invitrogen, Thermo Fisher Scientific, UK).

Peptide samples were vortexed with 2 µl Laemmli sample buffer (60 mM Tris-Cl pH 6.8, 2% SDS, 10% glycerol, 5% β-mercaptoethanol and 0.01% bromophenol blue) and heated at 100 °C for 10 minutes. The inner chamber of the electrophoresis cell was filled with 200 ml of running buffer (NuPAGE® MES SDS Running Buffer, 20X, Invitrogen, Thermo Fisher Scientific, UK) with the addition of 500 µl antioxidant (Invitrogen, Thermo Fisher Scientific, UK) to improve band separation. The outer chamber was filled with 600 ml of the same running buffer. Samples were run for approximately 90 minutes at 200 V (~100 mA) until they reached the bottom of the gel. Coomassie blue dye was used to stain the gel for 2-3 hours, assisted by orbital shaking. A destaining solution of methanol: acetic acid: water (5:4:1 v/v) was applied to the gel for 3-4 hours. Images of peptide bands were captured by high resolution photography (GelDoc-It ™, UVP, Cambridge, UK).

Western blot analysis was carried out using a standard wet blotting procedure on a 0.45 µm pore size membrane with a BenchMark® Pre-Stained protein standard ladder (Novex TM Thermo Fisher Scientific, UK). Electro-blotting was carried out for 1 hour at 200 V (~100 mA). Once protein transfer was finished, the membrane was removed and stained with Ponceau S solution (Sigma Aldrich, UK) for 3 minutes and then washed with distilled water, 0.1 M NaOH and Tris-buffered saline (TBS) buffer for 3 minutes each. A solution of 5% w/v of BSA in TBS buffer was added to nitrocellulose membrane with gentle shaking for 3 hours and then the membrane was incubated at 4 ºC overnight. The membrane was then washed twice with TBS buffer, before the addition of the primary antibody (guinea pig anti-human insulin IgG, 1:1000 dilution in TBS) for 3 hours at room temperature on an orbital shaker and then the membrane washed three times with TBS before the addition of the secondary antibody enzyme conjugate goat anti-guinea pig IgG alkaline phosphatase conjugate (1:30000 in TBS) for 3 hours at room

241 temperature with gentle shaking. Finally, the membrane was washed twice with TBS and
242 BCIP/NBT substrate solution added to the membrane to visualise protein bands.
243
244 *MALDI-TOF mass spectrometry*
245 MALDI-TOF MS equipped with a 1-minute time-of-flight tube was used in this study (Voyager-
246 DE Biospectrometer, PerSeptive Biosystems, Hertfordshire, UK). A 1.5 µl aliquot of insulin
247 standard solution (30 µl ml^{-1}) in 0.01 M HCL and insulin extracted from NP (obtained after the
248 digestion with 200 µl DCM and extraction into 500 µl 0.01 M HCL) were pipetted onto a
249 predefined well of a 100-well stainless-steel plate and allowed to dry at ambient temperature. A
250 10 mg ml^{-1} solution of α-cyano-4-hydroxycinnamic acid (CHCA, Fluka, Sigma Aldrich, UK)
251 was prepared in acetonitrile/ultrapure water/trifluoroacetic acid (80:20:0.1%). A 1.5 µl aliquot
252 of CHCA matrix was added to the sample spot and allowed to dry at ambient temperature. All
253 measurements were collected in linear positive ionisation mode using 50 laser shots per
254 spectrum. The accelerating voltage was maintained at 20 kV. The mass/charge ratio (m/z) was
255 plotted against relative abundance.
256
257 *2.9 Cell culture studies*
258 HaCaT and Hs27 cells were cultured in complete DMEM media supplemented with 10% FBS
259 and 1% Pen-Strep. Cells were incubated at 37 ºC and maintained in an atmosphere of 5% CO_2.
260 When cells reached 80–90% confluency, the media was aspirated and cells were washed with 15
261 ml PBS. Cells were then detached with 3 ml of 0.5 % trypsin-EDTA solution and incubated for
262 5 minutes. Trypsin was neutralised with complete media, and cells centrifuged at 10 rpm for 5
263 minutes, then resuspended in 10 ml of fresh complete media. Cells were counted by removing

10 µl of suspension and combining it with an equal volume of trypan blue solution. This mixture was vortexed, loaded into a haemocytometer chamber (Hawksley, UK) and counted visually (Primovet, ZEISS Industrial Company, Germany).

Cell culture scratch assay

A standard *in vitro* technique for detecting cell migration in two dimensions was used in this study. Known as a scratch assay or wound healing assay (WHA), it is based on formation of a cell-free region in a confluent monolayer by physical exclusion or by creating a cell-free gap through mechanical, thermal or chemical damage. HaCaT and Hs27 cell suspensions were diluted to 250,000 cells per ml in complete media and seeded into 24-well plates (Thermo Scientific, Korea) to a final well volume of 1.0 ml. Cells formed a confluent layer after 24 hours and then a double cross scratch was made using a sterile pipette tip. All wells were then washed twice with 1.0 ml PBS to remove cellular debris. A solution of free insulin (10^{-7} M) [26] and suspensions of insulin-loaded NP of variable PEG content containing 10^{-7} M insulin (Table1) were prepared in complete media (DMEM, 10% FBS and 1% Pen-Strep). Scratches were photographed and measured using bright field inverted microscopy at different time intervals depending on the rate of cell migration. The percent scratch closure at each time interval was normalised to the scratch length at the zero-time point. Wells containing 1.0 ml of complete media served as controls.

Cell viability assay

The effect of human insulin-loaded NP on cell proliferation was evaluated using an MTT assay, as described previously [27]. Briefly, cells (HaCaT or Hs27) were seeded in 96-well plates at an

initial density of 10000 cells per ml in complete DMEM medium. After 24 hours, the medium was replaced with 200 µl of fresh medium containing insulin-loaded NP (equivalent to 10^{-7} M insulin). Free insulin of equivalent concentrations was added as a control. The MTT assay was performed after predetermined time intervals of 12, 24 and 36 hours of incubation. Wells were photographed using bright field inverted microscopy. Cell viability was quantified by measuring absorbance at 590 nm (FLUOstar Omega, BMG LabTech, Germany) and compared to that of non-treated controls.

Uptake studies using dynasore hydrate

Dynasore, a cell permeable inhibitor, acts as a potent and rapid blocker of dynamin-dependent endocytic pathways by inhibiting coated vesicle formation [28]. To investigate the effect of dynasore additon on cellular uptake of NP, a stock solution (16 mM) of dynasore hydrate prepared in DMSO was diluted to 80 µM with DMEM. Cells (HaCaT or Hs27) were seeded in 96-well plates at an initial density of 10000 cells per ml in complete DMEM medium. After 24 hour of incubation, the medium was replaced with 100 µl of dynasore working solution (80 µM). After 30 minutes, the dynasore solution was replaced with either a suspension of insulin-loaded NP (FII) or free insulin solution (both equivalent to 10^{-7} M of insulin). The MTT assay was performed after 12 hour of incubation. To investigate the effect of a long-acting mechanism following prolonged dynasore exposure beyond the 30-minute interval, a second experiment was performed. Wells containing a mixture of dynasore solution and NP suspension (FII) were kept for 12 hours, while maintaining the concentration of dynasore and insulin at 80 µM and 10^{-7} M, respectively.

Cellular uptake imaging

Fluorescently-labelled, insulin-loaded NP (FII) were prepared using a modification of the technique detailed in section 2.2. Coumarin-6 was added (0.05% w/v) to the organic polymer solution prior to emulsification [29]. Cells ($1x10^5$ per well) were seeded on cover slips in a 6-well plate for 24 hours, then incubated with dynasore (80 µM) for 30 minutes to examine its inhibitory effect on cellular uptake of NP and then fluorescently labelled NP were incubated with cells for 24 hours. Cells not treated with dynasore were examined as a control. Cells were then washed with PBS, fixed with 4% formaldehyde for 30 minutes and re-washed with PBS. DAPI (5-10 µg ml^{-1}) was used to stain the nucleus. Cells were washed with PBS, suitably mounted and visualised using fluorescence microscopy (Eclipse 80i, Nikon Ltd., Japan).

2.10 Statistical analysis

Data are presented as the mean ± standard deviation (SD). A Student's t-test and one-way analysis of variance (ANOVA) were used to determine significance between groups. *Post hoc* analysis using Tukey's HSD test was used to compare the means of individual groups. A value of $p<0.05$ was considered to be significant.

3. Results and Discussion

3.1. Particle size and zeta potential measurements

Creating a PEG-rich periphery on a NP serves many functions, besides the more customary attempt to increase residence time in the systemic circulation [30]. PEG is associated to NP via different methods that include covalent bonding, direct addition during NP preparation or surface adsorption. In this study, the second approach was adopted, which gives rise to a particulate surface that reduces opsonisation [31]. This protein adsorption can be minimised further by altering the density and molecular weight of PEG, a variation that was used in this study (Table 1). The data in this table show that addition of lower molecular weight (2 kDa) PEG had a significant effect ($p<0.05$) on particle size, whereas the higher molecular weight (5 kDa) type had a lesser effect. It has been shown that the addition of PEG modifies the association of polymers during the formation of NP, which leads to a decrease in the resulting particle size, as observed in this work [32].

Various methods have been described for characterising the extent of surface charge shielding provided by PEG on the surface of NP [30]. Here, we found that increasing PEG content (density and/or molecular weight) had no significant effect on zeta potential. This finding is explained by the choice of method used to add PEG into the nanoparticle matrix. In this work, PEG does not form a covalent part of the polymeric structure, which is in contrast to PEG in NP constructed from PEG-PLGA co-blocks, which do show evidence of attenuated surface charge.

3.2. Drug loading (DL) and entrapment efficiency (EE)

Addition of PEG led to a significant increase in DL and direct EE (%) with a greater effect observed following use of the lower molecular weight PEG (2 kDa) ($p<0.05$). During the double-emulsion-based nano-encapsulation process, it is feasible that PEG chains assemble at the interface between the peptide-containing internal phase and the organic phase. This effect prevents peptide from migrating towards the external aqueous phase, which may explain the higher encapsulation efficiencies [33].

The choice of method used to measure entrapment efficiency had a bearing on the estimate of entrapped drug. Determination of EE (%) using direct and indirect methods resulted in higher values when the indirect EE method was compared to the direct EE ($p<0.05$) method. The indirect method for estimating EE (%) depends on detecting drug concentration in the supernatant and is, therefore, not a direct measure of particulate loading. Indeed, further processing, such as washing and centrifugation, will remove loosely bound drug and so a preliminary analysis of the supernatant immediately following NP formation may be an overestimation. Although significantly different, the data in Table 1 show reasonably good agreement between both methods and so it can be concluded that the incorporated insulin is firmly associated or entrapped within the NP and not loosely bound to its surface.

3.3. In vitro release kinetics

In vitro release profiles (Fig. 1) showed an initial burst release followed by a sustained release phase over 144 hours. There are key factors that affect the release profile of NP. Larger particles have a smaller initial burst release and longer sustained release than smaller particles. In addition, higher drug loadings typically produce a higher initial burst and a faster release rate [31]. The addition of PEG resulted in a significant increase in the initial release burst and the

overall % cumulative release over 6 days ($p<0.05$) for FII, FIII and FIV compared to F1. FII exhibited the maximum % cumulative release of approximately 70% (w/w). Formulations containing PEG (FII-FIV) had greater drug loadings, which resulted in higher initial burst releases (Fig. 1). This initial finding is explained by rapid diffusion of peptide close to the surface of the NP, which was enhanced by the addition of PEG [30]. Furthermore, an increase in the porosity of the NP is expected, caused by the presence of PEG in the polymeric phase of the preparation emulsion [34].

3.4. Morphological characterisation

NP displayed a spherical geometry with smooth surfaces (Fig. 2). The effect of adding PEG, as represented by FII, decreased particle size and tightened its distribution (Fig. 2C-D), compared with FI that had no PEG in the primary emulsion (Fig. 2A-B). Samples that had undergone 48 hours of release were examined using microscopy to determine the residual appearance following drug extraction (Fig. 2E-G). We found in this current work that the initial burst release in the first 24 hours was attributed to diffusion of the drug bound to the surface of the NP and the succeeding sustained release phase was due to gradual erosion of the polymer matrix (Fig. 2E-G). This mechanism aligns to the theoretical mechanisms of drug release proposed by Danhier *et al*., comprising a combined erosion–diffusion process [35].

3.5. In vitro drug stability

Maintaining the stability of a model payload during the release phase from NP is a key requirement. Specifically, the risk of peptide degradation or aggregation during NP fabrication is a problem and should be monitored and characterised. High rates of shear produced during

395 homogenisation of primary and secondary emulsion phases lead to three-dimensional alternation
396 in peptide structure [36]. Therefore, in this work, insulin stability was assessed using the
397 recombinant human insulin molecule (5.8 kDa) as an indicator of peptide integrity.

398 SDS-PAGE and western blot were used to compare the position of insulin bands obtained
399 from a (i) standard control, (ii) insulin released from NP and (iii) a placebo NP sample with no
400 insulin loading. Bands in Fig. 3 confirm that both the insulin standard and the insulin released
401 from loaded NP have an approximate molecular weight of 6.00 kDa. Another method used to
402 determine the stability of entrapped insulin was to compare its molecular weight, following
403 release, to that of an insulin standard. The mass spectra in Fig. 4A and 4B demonstrate close
404 agreement between peak values, confirming that entrapped insulin did not suffer aggregation or
405 degradation following NP processing or *in vitro* release.

406

407 *3.6. Cell culture of human skin cell line*

408 Scratch assays were performed using HaCaT and Hs27 cells to investigate the bioactivity of
409 insulin-loaded PLGA NP. Compared to other methods, the *in vitro* scratch assay is particularly
410 suitable for mimicking cell migration during *in vivo* wound healing and is compatible with
411 imaging of live cells during migration to monitor intracellular events [37]. Fronza *et al*. [38] and
412 Hrynyk *et al*. [26] used *in vitro* scratch assays in their work to measure cell migration across the
413 scratch as a viable method for quantification of wound closure.

414 The mean width of the applied scratch was 1.18 mm (average of six measurements between
415 the four edges of the cross scratch), which started to close due to cell migration, stimulated by
416 applied insulin (Fig. 5). The amount of insulin (free or encapsulated in NP) applied to the cell
417 scratch at the beginning of the assay was equivalent to 10^{-7} M for all conditions, with the

418 exception of control media (complete DMEM) and placebo NP (0% insulin control), in which
419 case PLGA degradation products were assayed to determine if they had a migration response on
420 cells. Fig. 6 represents assays of different NP formulations, as displayed in Table 1, on HaCat
421 cells (Fig. 6A) and Hs27 cells (Fig. 6B).

422 Migration is considered a normal pattern of behaviour for HaCaT cells, but the differences
423 between cells exposed to insulin-loaded NP and those growing in the absence of insulin or
424 exposed to free insulin were significantly different. This is evident after 24 hours and 36 hours
425 (Fig. 6A). Cells exposed to insulin NP formulations (FII-FIV) formed a confluent monolayer at
426 24 hours. At 36 hours, the percentage scratch closure was 96.7% for cells exposed to FII in
427 comparison to 64.8% and 69.6% for cells exposed to DMEM and free insulin, respectively.
428 Similar results were found for Hs27 cells. At 48 hours, the percentage scratch closure was
429 87.9% for cells exposed to FII in comparison to 53.0% and 18.2% for cell migration data
430 following exposure to control DMEM and free insulin, respectively. Most of the wells exposed
431 to insulin-loaded NP formulations (FII-FIV) formed a confluent monolayer at 36 hours.

432 The short-term effect of all NP formulations on Hs27 was less pronounced than that observed
433 on the HaCaT cell line. For this reason, the total time for the scratch assay was extended to 48
434 hours so that effects on migration were more clearly seen (Fig. 6B). Free insulin had a negative
435 effect on migration when compared to control DMEM and placebo NP ($p<0.01$). As shown in
436 Fig. 6B, NP formulations with PEG content (FII-FIV) had a significant effect on cell migration
437 ($p<0.05$) compared to FI (no PEG content) or FV (NP with high density and high PEG molecular
438 weight). These results demonstrated that if cellular migration was dependent on effective insulin
439 delivery, then nano-encapsulation was a more efficient approach when compared to direct
440 exposure of the free drug. This suggested that particulate uptake was playing a role in the results

observed in this work. The addition of PEG to the NP formulations lends weight to this argument in that it can enhance cellular uptake due to a smaller resultant NP size [39].

3.6.2. MTT cell assay (Cell viability)

In this work, the MTT assay was used to evaluate cell proliferation [40] and results demonstrated the proliferative effect of insulin-loaded NP, which exhibited a more pronounced effect on HaCaT cells ($p<0.001$) when compared to Hs27 cells ($p<0.05$). For HaCaT cells (Fig. 7A), insulin-loaded NP extended the proliferative effect for 36 hours (Table 2(a)). For example, at 36 hours, FIII showed a % cell viability of 112.88 %, whereas free insulin and placebo NP showed % cell viability of 99.80 % and 98.38%, respectively. The results were different for Hs27 cells, as seen in Table 2(b). The maximum proliferation effect of insulin-loaded NP was observed at 12 hours, with no significant difference at 24 and 36 hours (Fig. 7B). For example, at the 12-hour time point, FIII showed % cell viability of 115.98%, whereas free insulin and placebo NP showed % cell viability of 100.18% and 102.82%, respectively.

3.6.3. Effect of dynasore hydrate on cellular uptake of Insulin-NP

As demonstrated in Fig. 8A and 8B, the addition of dynasore hydrate led to a significant decrease in cell proliferation for HaCaT cells ($p<0.02$) and Hs27 ($p<0.05$). This was attributed to the inhibitory effect of dynasore, which blocks the endocytic pathways responsible for NP uptake. HaCaT cell proliferation data for free insulin, control DMEM and insulin-loaded NP after the addition of dynasore for 30 minutes showed that although dynasore exerts its inhibitory effect on NP uptake, we found that % cell proliferation of free insulin and insulin-loaded PLGA NP was significantly ($p<0.03$) higher than control DMEM, with no significant difference observed

464 between free insulin and insulin-loaded NP. These results support the argument that insulin-
465 enhanced migration of HaCaT cells via NP translocation passively through the cell membrane
466 [41] in addition to active cellular uptake, which is blocked in the presence of dynasore. This is in
467 agreement with the work of many, such as Wang et al. [42] who propose that NP uptake is done
468 actively by cellular uptake machinery or by passive penetration. During endocytosis, NP are
469 enclosed by endocytic vesicles and are, thus, not directly transferred into the cytosol. By
470 contrast, NP internalised by membrane penetration enter the cytosol directly, which can be
471 preferable for targeted drug delivery. Therefore, the interaction of NP with the cell membrane
472 depends on the physical properties of NP and cell membrane structure [42].

473 Hs27 cell proliferation data, as seen in Fig. 8B, showed that addition of dynasore for 30
474 minutes led to inhibition of cell migration with no significant difference observed between free
475 insulin, insulin-loaded NP and the control (DMEM). These results mean that the migration
476 effect of insulin on Hs27 is largely dependent on an active endocytic pathway. The most
477 pronounced proliferation effect occurred after insulin-loaded NP application in the absence of
478 dynasore. Generally, incubation of HaCaT and Hs27 cells in the presence of dynasore for a
479 longer time duration (12 hours) led to significant increases in cell growth, as shown in Fig. 8A
480 and 8B. Dynasore is a newly identified inhibitor of dynamin GTPase activity, which arrests the
481 progression of endocytosis at coated-pit stages, inhibits internalisation of cell-surface-bound
482 TGFβ and promotes co-localisation and accumulation of TβR-I and SARA at the plasma
483 membrane. Therefore, dynasore is considered to be a potent enhancer of TGFβ, which
484 stimulates cell growth and may explain the call viability patterns at prolonged time intervals
485 [43].
486

3.6.4. Cellular uptake imaging (fluorescence microscopy)

In this study, coumarin 6 was chosen as a fluorescence label in fluorescence imaging microscopy due to its low dye-loading requirement [44]. It is observed in Fig. 9A and 9C that the fluorescence of the coumarin-6 loaded NP (green) are closely located around the nuclei (blue stained by DAPI), which indicates that the NP have been taken up by the cells, after 24-hour incubation. Obviously, cells treated with dynasore have a lower cellular uptake efficiency as it is shown in Fig. 9B and 9D. This result further supports the contention that dynasore was blocking endocytic process responsible for NP uptake [28].

4. Conclusion

Recombinant human insulin was encapsulated into PLGA NP by a W/O/W solvent evaporation technique with high efficiency and reproducibility. Release studies demonstrated that insulin was delivered for 6 days in a sustained release manner. Furthermore, an *in vitro* scratch assay established that insulin released from PLGA NP stimulated rapid cell migration following an induced scratch. Furthermore, MTT assay results confirmed that insulin could enhance cell proliferation, particularly if nano-encapsulated. Blockage of endocytic pathways verified that particulate uptake was responsible for the enhanced cellular response that surpassed that observed with exposure to free insulin. These data suggest that insulin encapsulated within PLGA NP offers potential for long-term delivery of bioactive insulin for topical delivery devices and could have significant clinical implications for the treatment to poorly responsive chronic wounds.

Acknowledgment

The authors would like to acknowledge financial support from the cultural affairs and mission sector, Egyptian government, Egypt.

513 **Fig. 1.**

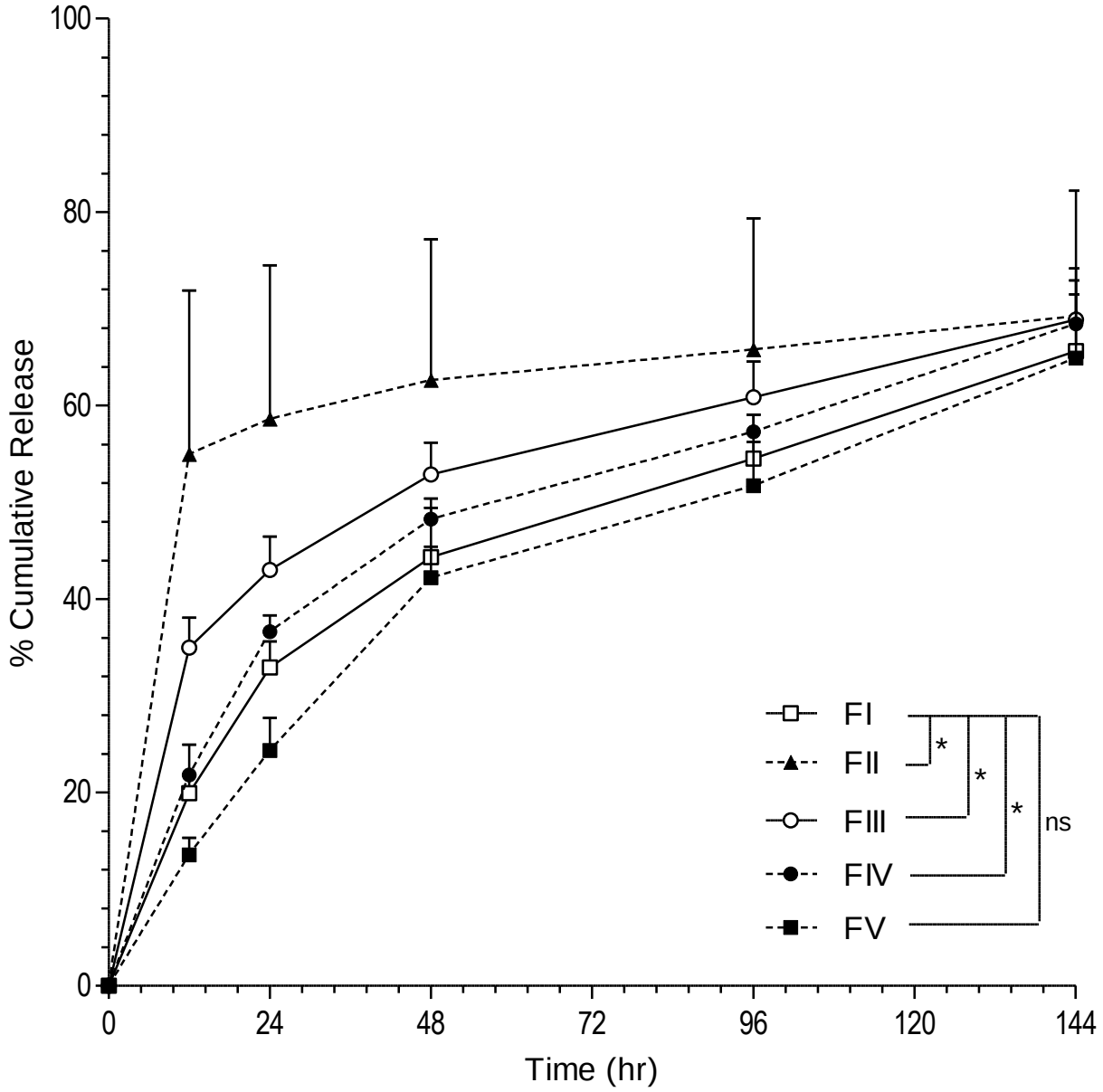

514
515

516 Fig 1. *In vitro* drug release profiles from insulin-loaded PLGA NP (Formulation codes shown in
517 Table 1). For clarity, data are shown as mean + SD (n=3). Single asterisks indicate statistical
518 significance ($p < 0.05$) between (FII-FIV) and FI, ns (non-significant difference) between FV
519 and FI.
520

Fig. 2.

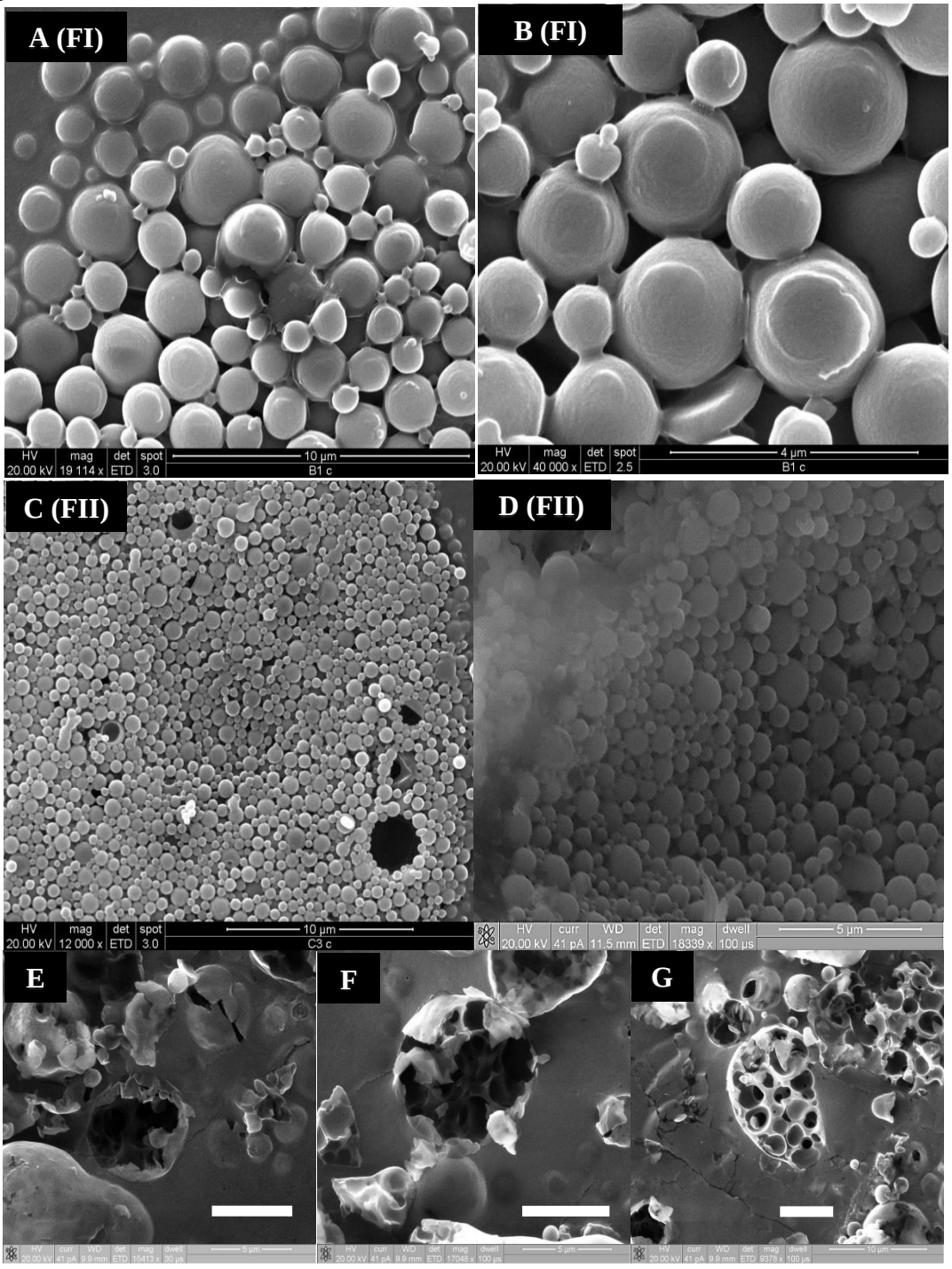

Fig 2. Scanning electron micrographs of insulin-loaded NP prepared with PEG (FII) and without PEG (FI), observed under low magnification (A and C) and at higher magnification (B and D). Images in E-G show polymeric structures (FII) with voids following exposure to release phase media. Bars in E, F and G represent 5 μm.

Fig. 3.

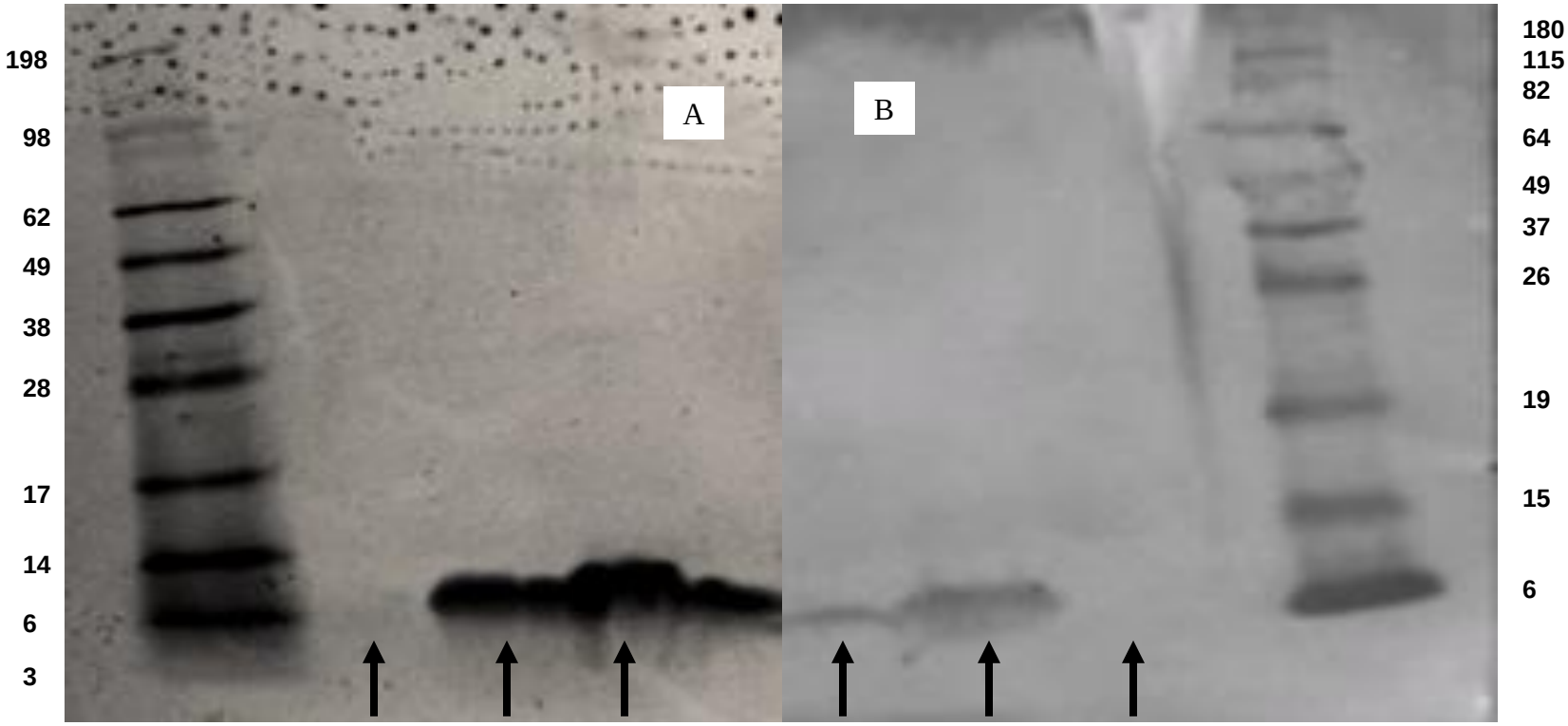

Fig. 3. *In vitro* stability of human insulin released from NP as assessed from (A) SDS-PAGE and (B) western blot. Ladders indicate molecular weight in kDa. Lane 1 – blank NP. Lane 2 – insulin released from NP. Lane 3 – control insulin. Lane 4 – insulin released from NP. Lane 5 – control insulin. Lane 6 – blank NP.

Fig. 4A.

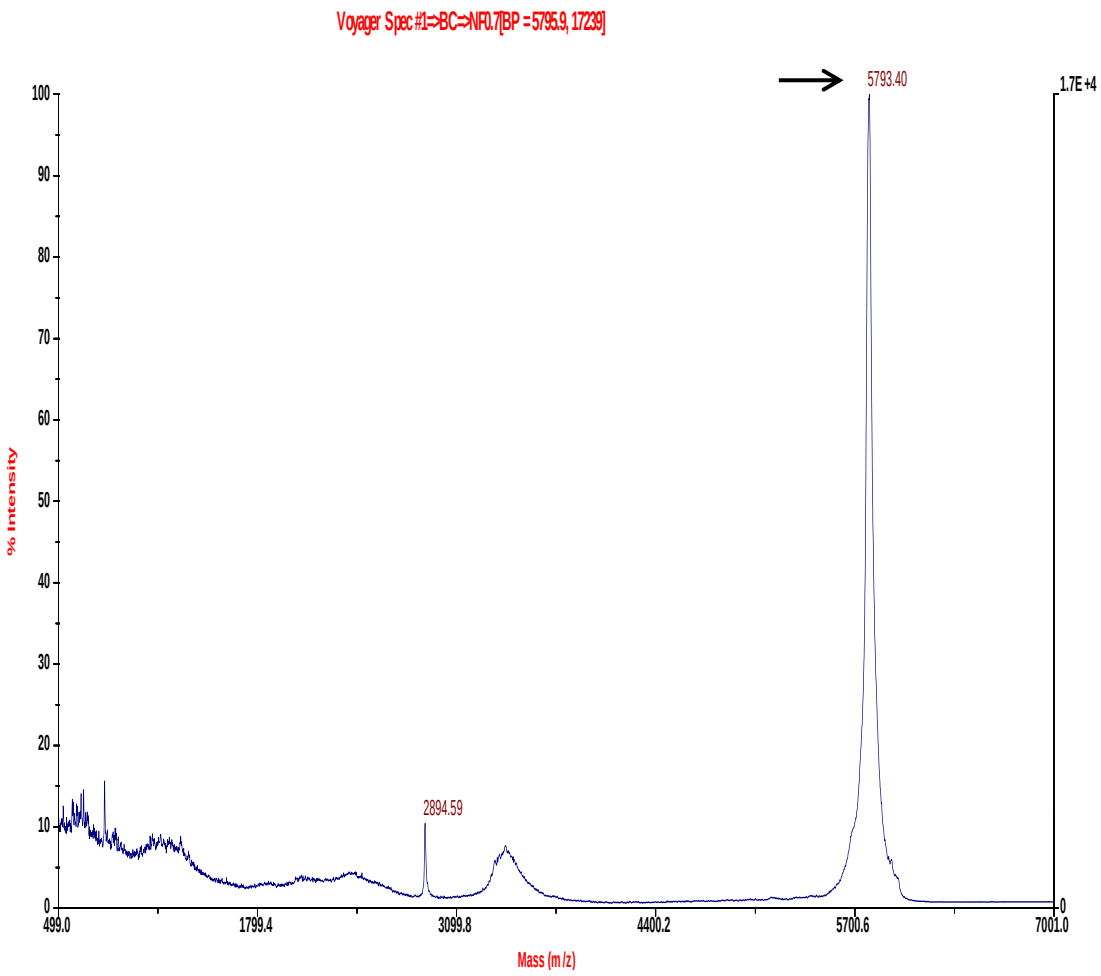
Voyager Spec #1=>BC=>NF0.7[BP = 5795.9, 17239]
5793.40
1.7E+4
2894.59
% Intensity
Mass (m/z)
100
90
80
70
60
50
40
30
20
10
0
499.0
1799.4
3099.8
4400.2
5700.6
7001.0

Fig. 4B.

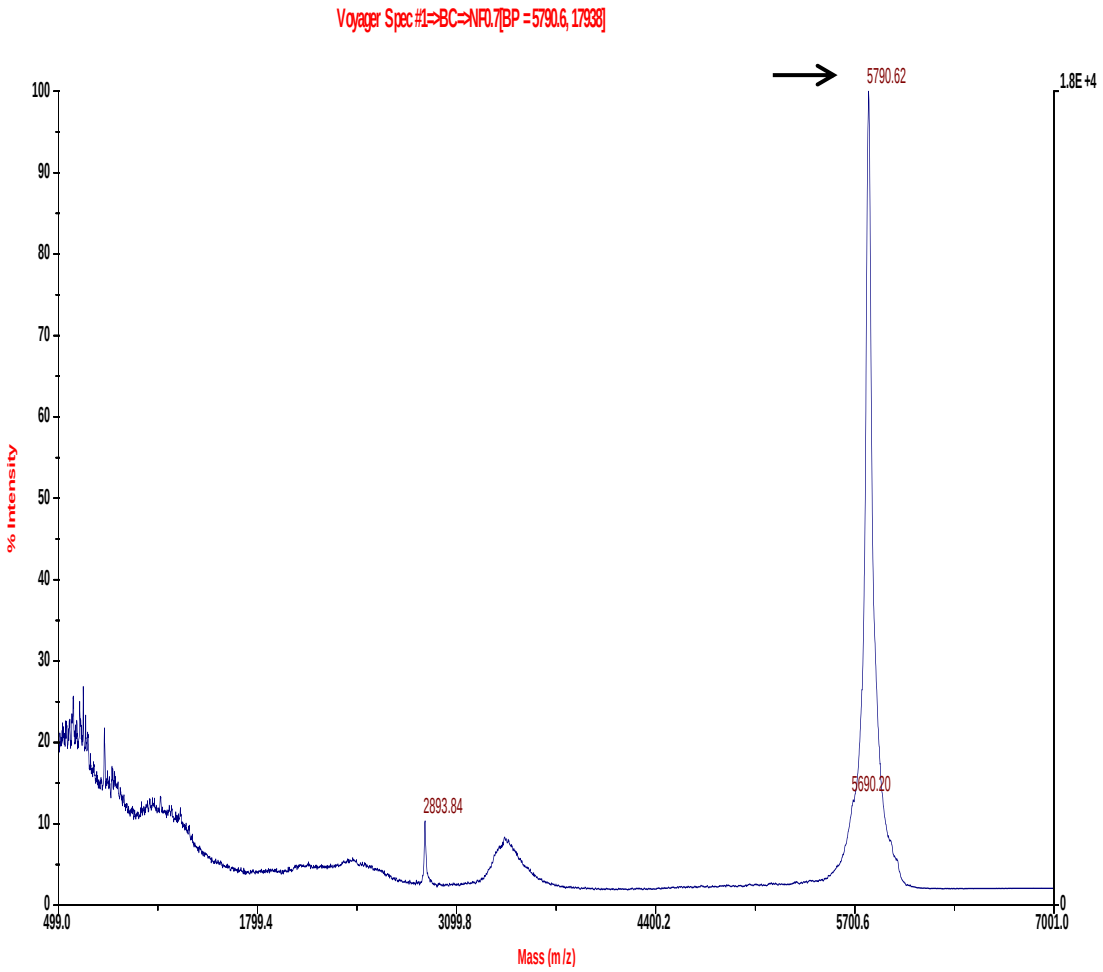

Fig 4. MALDI-TOF mass spectrum of (A) an insulin standard and (B) insulin released from NP.

Fig. 5A

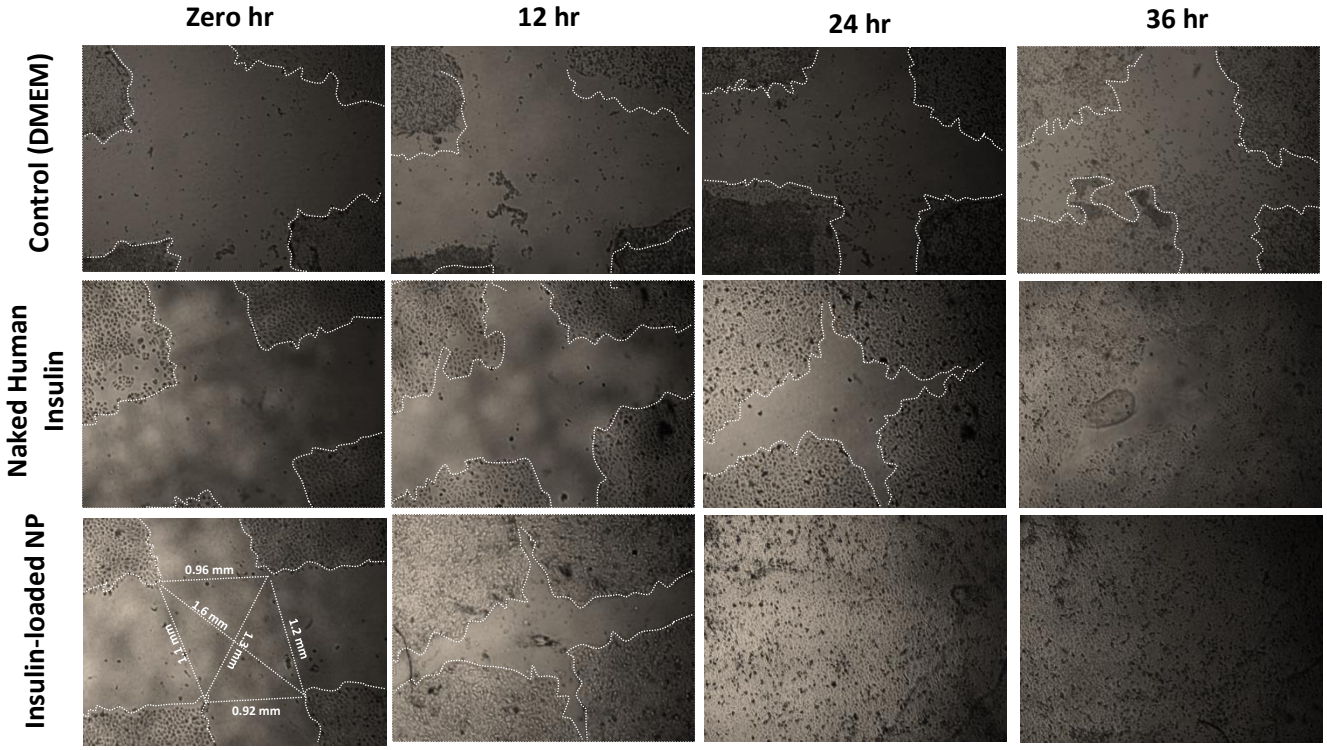

Fig 5A. Representative images of the HaCaT cell line showing the scratch closure process following treatment with DMEM control, free insulin and insulin-loaded NP (FII) at different time intervals of zero, 12, 24 and 36 hours. Scratch dimensions, as illustrated in the panel for insulin-loaded NP at zero time, were determined using ImageJ software. The advancing cell border is highlighted using a dashed line.

Fig. 5B.

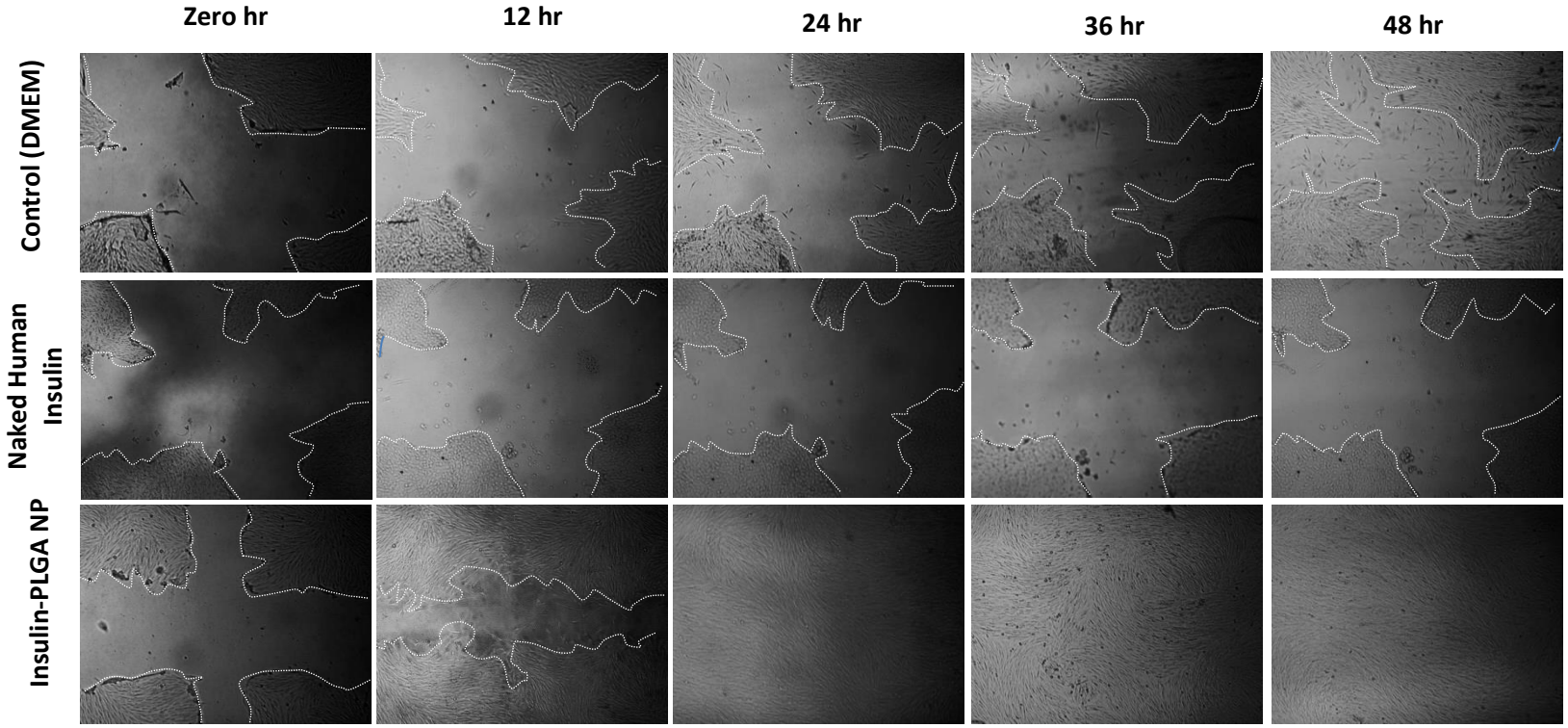

Fig. 5B. Representative images of scratch closure with respect to time for Hs27 cells following treatment with a control (DMEM), free insulin and insulin-loaded NP (FII).

Fig. 6A.

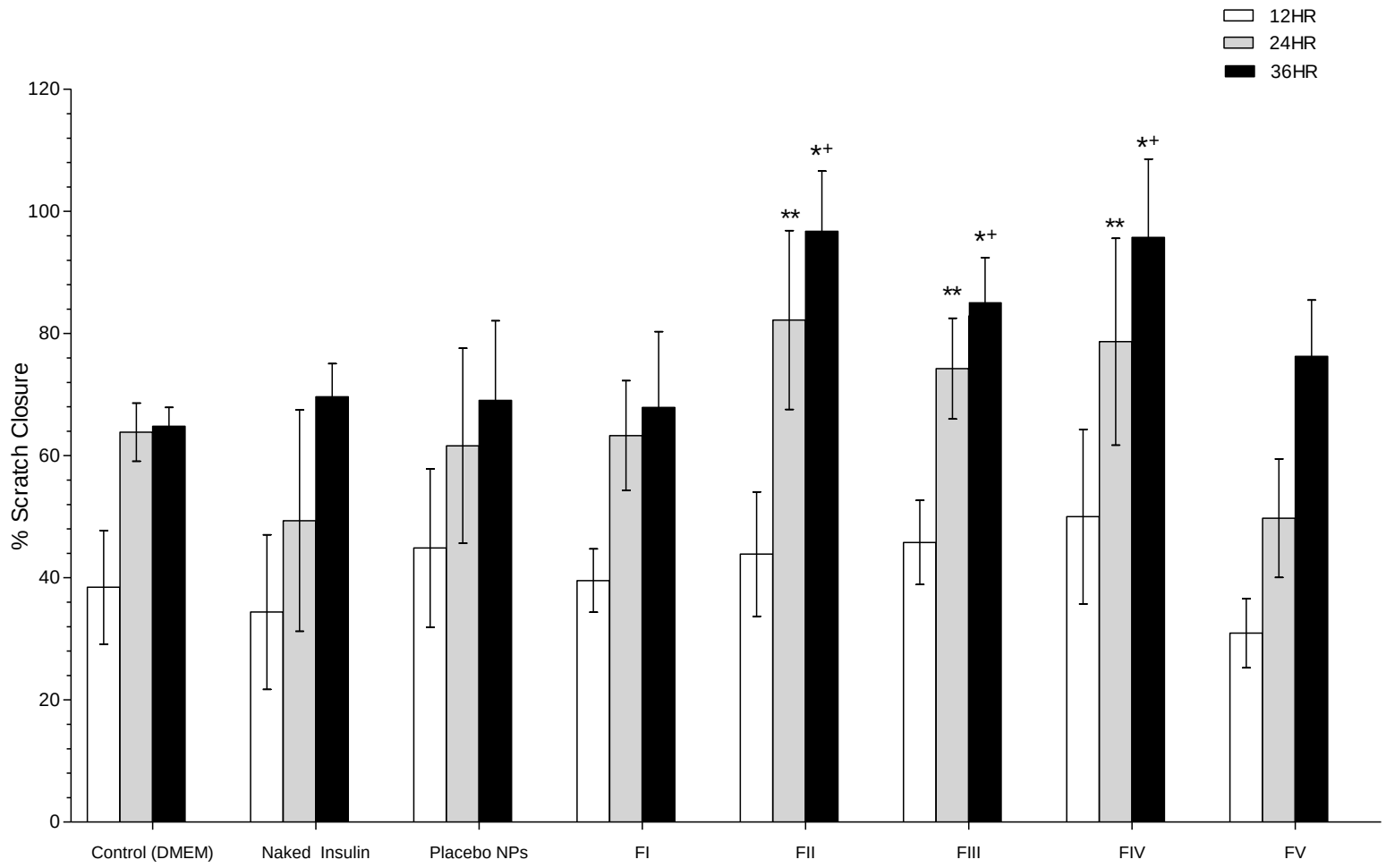

Fig. 6A. HaCaT cell scratch closure assay evaluating bioactivity of recombinant human insulin released from PLGA NP.

Fig. 6B.

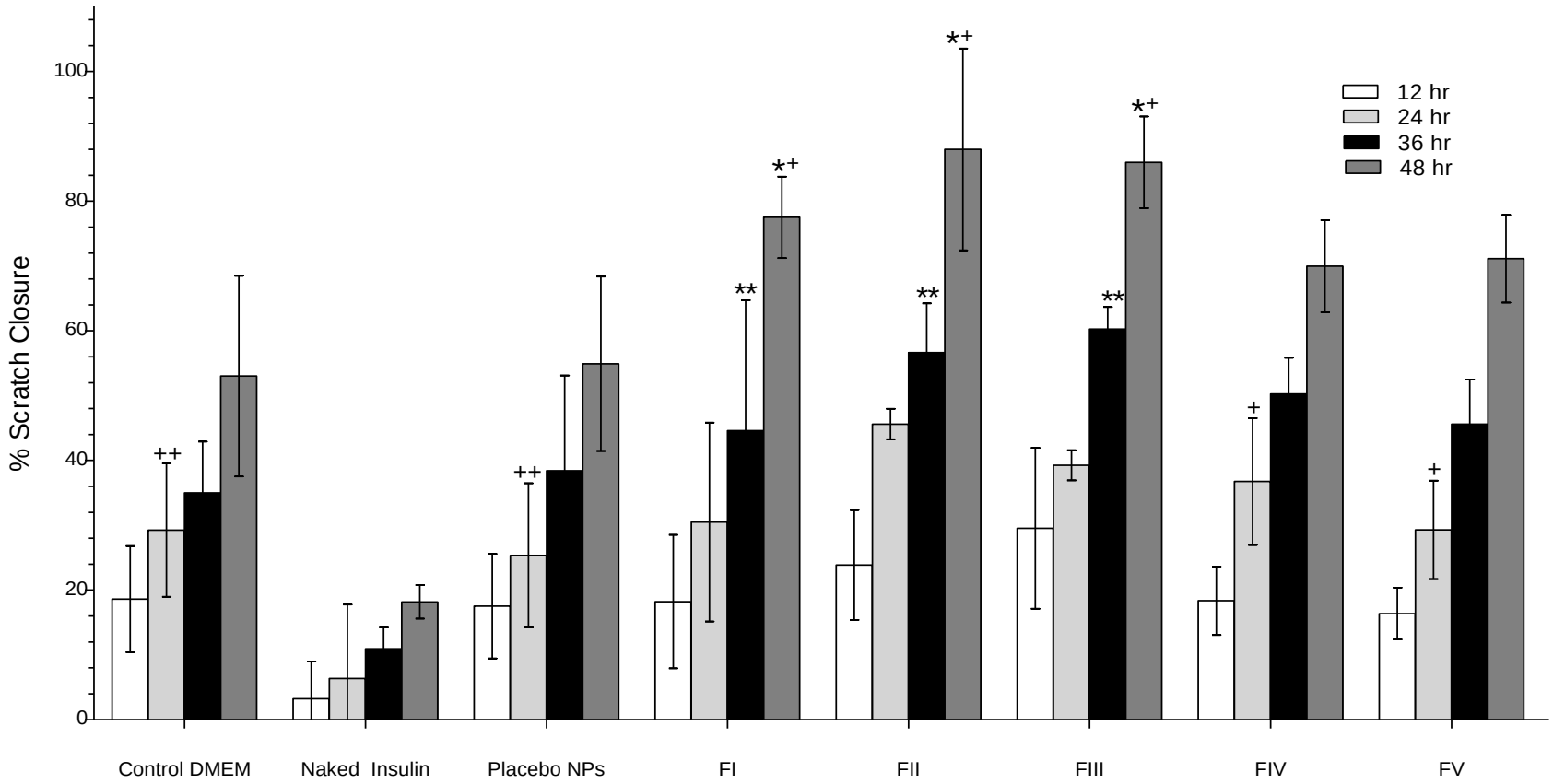

Fig 6B. Hs27 cell scratch closure assay evaluating bioactivity of recombinant human insulin released from PLGA NP. Single asterisks indicate statistical significance between control (DMEM) and insulin-loaded NP. ** and *+ indicates statistical significance between placebo NP and insulin-loaded NP, + indicates statistical significance between free (naked) insulin and insulin-loaded NP; ++ indicates statistical significance between free (naked) insulin and placebo NP. Results are mean ±SD of nine replicates.

Fig. 7A.

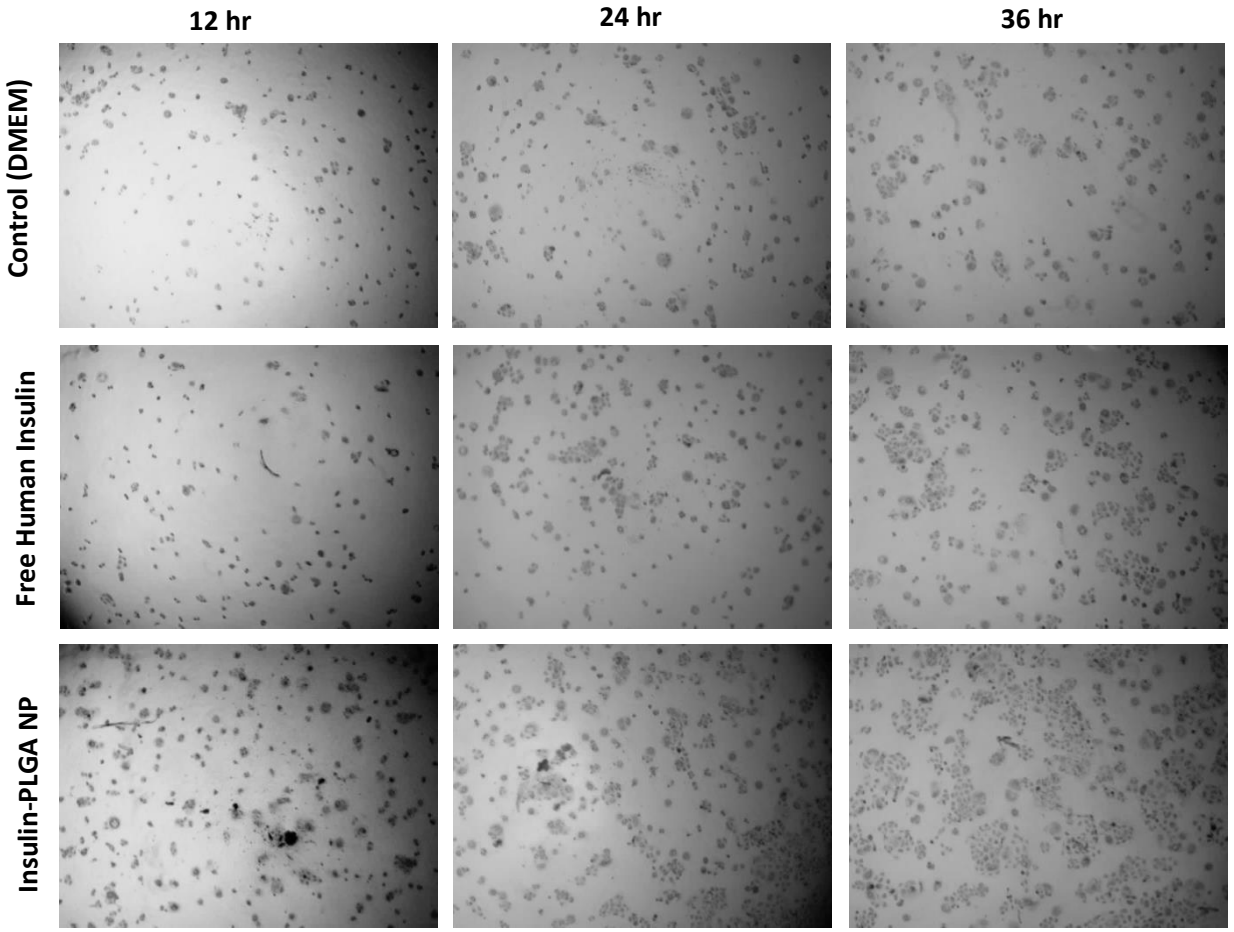

Fig 7A. Representative images of HaCaT cell line showing cell proliferation, measured by MTT assay, treated with control, naked insulin and insulin-loaded NP (FII) at different time intervals of 12, 24 and 36 hours, respectively.

Fig. 7B.

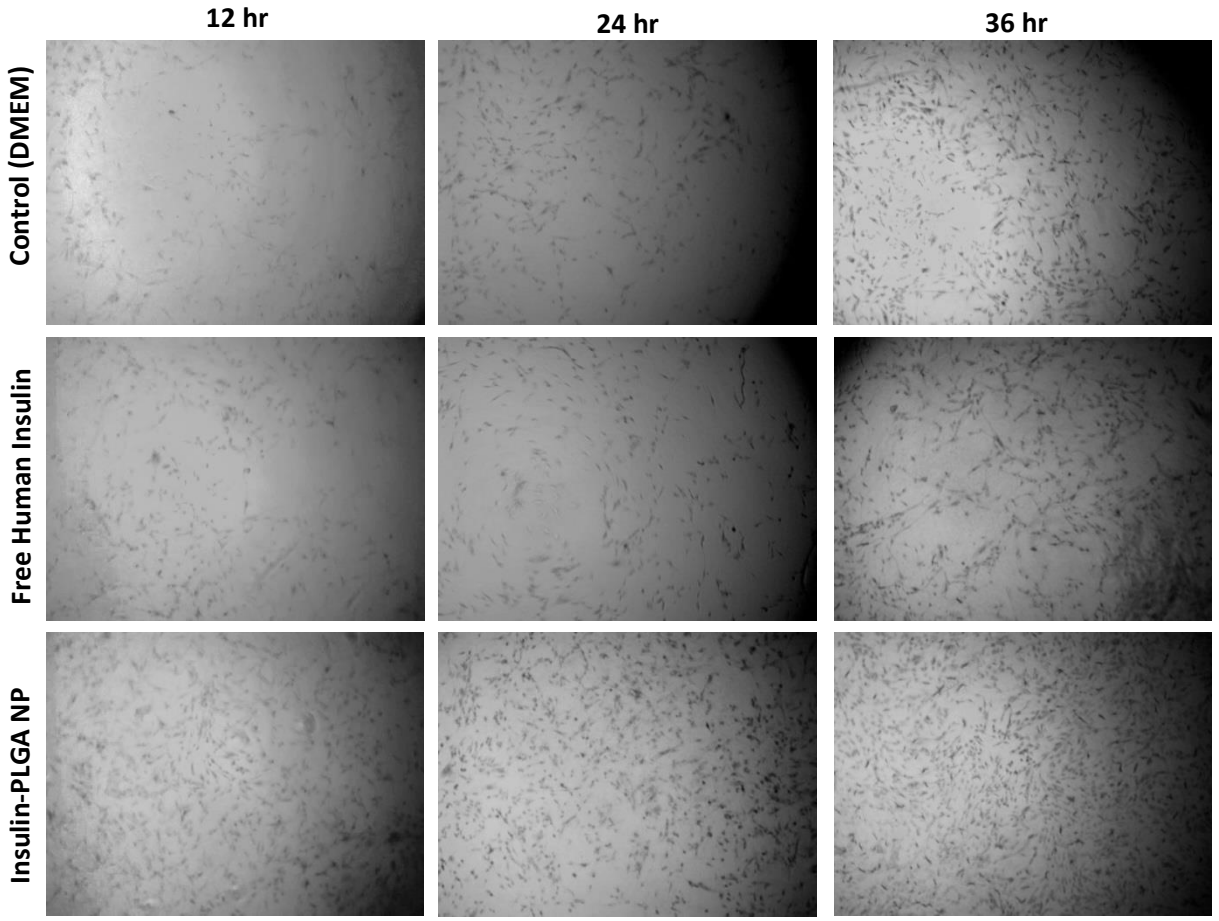

Fig. 7B. Representative images of Hs27 cell line showing cell proliferation, measured by MTT assay, treated with control, free insulin and insulin-loaded NP (FII) at different time intervals of 12, 24 and 36 hours, respectively.

Fig. 8A.

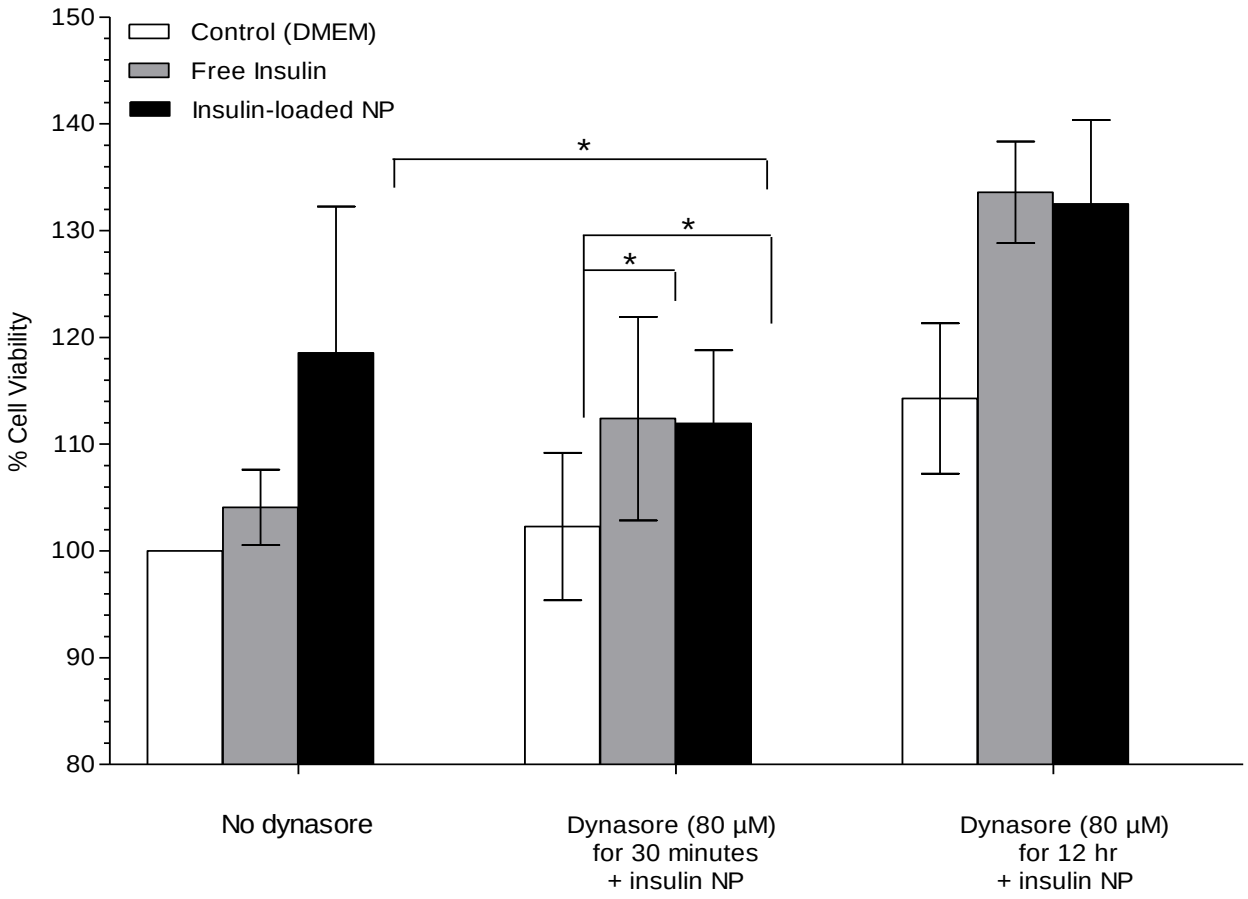

Fig. 8A. Evaluation of HaCaT cell viability (%) , measured by MTT assay, following treatment with control, free insulin and insulin-loaded NP (FII) showing the inhibitory effect of dynasore exposure. Between groups significance indicated by * ($p<0.02$).

Fig. 8B.

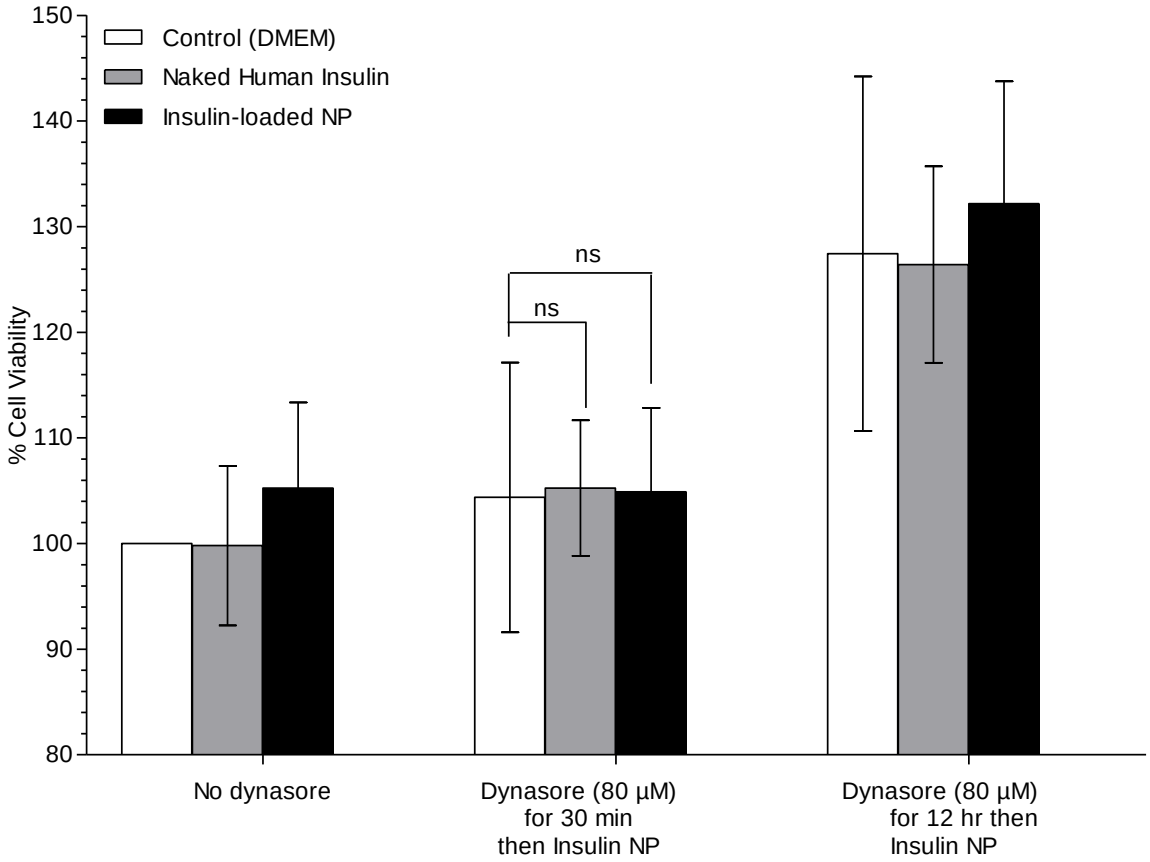

Fig 8B. Hs27 cell viability (%), measured by MTT assay, treated with control, free insulin and insulin-loaded NP (FII) showing the inhibitory effect of dynasore. Between groups ANOVA Results showed no significant difference (ns).

Fig. 9.

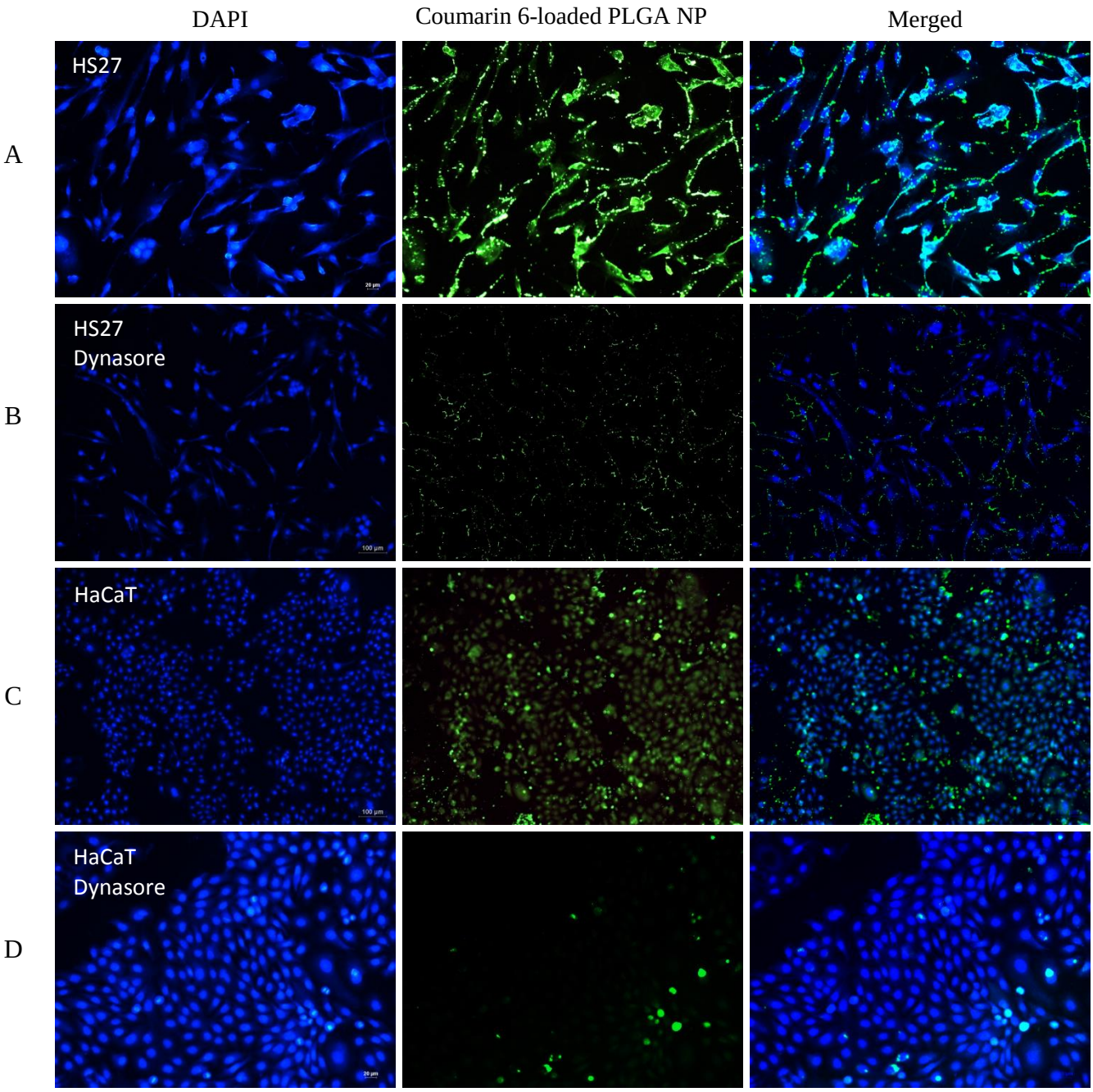

Fig 9. Fluorescence imaging microscopy of HS27 cells (A, B) and HaCaT cells (C, D) after incubation for 24 hours at 37 °C with coumarin 6-loaded NP (modified FII). A and C are control images (absence of dynasore), B and D are images of cells treated with dynasore (80 μM) for 30 minutes before addition of coumarin 6-loaded NP.

Table 1.

Effect of PEG content on size, charge and drug entrapment data for insulin-loaded PLGA NP

Formula code	PEG content in primary emulsion M_w (% w/w)	Z-average (nm)	PDI	Zeta potential (mV)	Drug loading µg per mg NP	Direct EE (%)*	Indirect EE (%)†
FI	----	297.8±18.8	0.15±0.02	-3.94±0.02	28.47±5.35	56.9±10.7	69.1±0.6
FII	2 kDa (5%)	202.6±20.6	0.38±0.06	-5.70±0.17	33.86±2.71	67.7±5.4	69.5±3.3
FIII	2 kDa (10%)	186.9±26.0	0.26±0.04	-5.75±0.03	35.60±3.84	71.2±7.6	69.6±5.6
FIV	5 kDa (5%)	243.5±45.5	0.35±0.03	-7.52±0.07	31.73±4.14	63.4±8.2	73.7±3.2
FV	5 kDa (10%)	255.6±28.9	0.38±0.02	-8.76±0.17	30.26±4.91	60.5±9.8	69.7±3.0

Data represent mean ± SD of three replicates. *Direct entrapment efficiency (EE) measured by BCA †Indirect EE measured by HPLC.

Table 2(a)

Percent cell viability of HaCat cells treated with insulin-loaded NP at three time points over 36 hours

Treatment	% Cell Viability		
	12 hours	24 hours	36 hours
Control (DMEM)	100.00±0.00	100.00±0.00	100.00±0.00
Naked Human insulin	98.12±4.19	104.22±6.01	99.80±8.63
Placebo NP	115.32±5.86	105.35±5.41	98.38±9.97
FI	115.83±5.05	107.56±10.61	110.28±4.84
FII	114.88±6.79	104.49±6.22	102.12±7.43
FIII	122.77±10.58	111.80±7.09	112.88±7.98
FIV	118.43±7.20	110.26±5.67	107.06±9.05
FV	124.38±5.55	110.63±4.82	114.82±5.50

* results show mean±SD of six replicates

Table 2(b)

Percent cell viability of Hs27 cells treated with insulin-loaded NP at three time points over 36 hours

Treatment	% Cell Viability*		
	12 hours	24 hours	36 hours
Control (DMEM)	100.00±0.00	100.00±0.00	100.00±0.00
Naked Human insulin	100.18±10.24	100.92±5.88	101.96±13.46
Placebo NP	102.82±12.97	104.25±14.73	107.51±13.01
FI	111.73±8.18	103.63±13.60	111.32±17.79
FII	114.00±16.64	104.35±6.07	104.57±11.84
FIII	115.98±16.00	103.68±3.79	105.98±14.71
FIV	107.45±15.73	114.74±5.37	114.23±18.00
FV	108.80±16.92	108.26±8.93	100.91±13.32

* results show mean±SD of six replicates

References

[1] M. Hrynyk, R.J. Neufeld, Insulin and wound healing., Burns. 40 (2014) 1–14. doi:10.1016/j.burns.2014.03.020.

[2] V. Falanga, Wound healing and its impairment in the diabetic foot, Lancet. 366 (2005) 1736–1743. doi:10.1016/S0140-6736(05)67700-8.

[3] Y. Liu, M. Petreaca, M. Yao, M. Martins-Green, Cell and molecular mechanisms of keratinocyte function stimulated by insulin during wound healing., BMC Cell Biol. 10 (2009) 1–15. doi:10.1186/1471-2121-10-1.

[4] S.P. Rosenthal, Acceleration of primary wound healing by insulin., Arch. Surg. 96 (1968) 53–55. doi:10.1001/archsurg.1968.01330190055012.

[5] K.N. Udupa, J.P. Chansouria, The role of protamine zinc insulin in accelerating wound healing in the rat., Br. J. Surg. 58 (1971) 673–675.

[6] Abdelkader DH, Osman MA, El-Gizawy SA, Faheem AM, McCarron PA,The Role of Insulin in Wound Healing Process : Mechanism of Action and Pharmaceutical Applications, J. Anal. Pharm. Res. 2 (2016) 1–6. doi:10.15406/japlr.2016.02.00007.

[7] M.H.M. Lima, A.M. Caricilli, L.L. de Abreu, E.P. Araújo, F.F. Pelegrinelli, A.C.P. Thirone, D.M. Tsukumo, A.F.M. Pessoa, M.F. dos Santos, M. a. de Moraes, J.B.C. Carvalheira, L. a. Velloso, M.J. a Saad, Topical insulin accelerates wound healing in diabetes by enhancing the AKT and ERK pathways: A double-blind placebo-controlled clinical trial, PLoS One. 7 (2012) 1–13. doi:10.1371/journal.pone.0036974.

[8] R.A.N. Achar, T.C. Silva, E. Achar, R.B. Martines, J.L.M. Machado, Use of insulin-like growth factor in the healing of open wounds in diabetic and non-diabetic rats., Acta Cir.

Bras. 29 (2014) 125–31. doi:10.1590/S0102-86502014000200009.

[9] E. Wang, M. Zhao, J. V. Forrester, C.D. McCaig, Electric fields and MAP kinase signaling can regulate early wound healing in lens epithelium, Investig. Ophthalmol. Vis. Sci. 44 (2003) 244–249. doi:10.1167/iovs.02-0456.

[10] I. D.Goldfine, Insulin receptors and the site of action of insulin, Life Sci. 23 (1978) 2639–48. doi:https://doi.org/10.1016/0024-3205(78)90643-4.

[11] S.S. Guterres, M.P. Alves, A.R. Pohlmann, Polymeric nanoparticles, nanospheres and nanocapsules, for cutaneous applications., Drug Target Insights. 2 (2007) 147–157.

[12] Z. Zhang, P.-C. Tsai, T. Ramezanli, B.B. Michniak-Kohn, Polymeric nanoparticles-based topical delivery systems for the treatment of dermatological diseases, Wiley Interdiscip. Rev. Nanomedicine Nanobiotechnology. 5 (2013) 205–218. doi:10.1002/wnan.1211.

[13] A. Taluja, Y.S. Youn, Y.H. Bae, Novel approaches in microparticulate PLGA delivery systems encapsulating proteins, J. Mater. Chem. 17 (2007) 4002. doi:10.1039/b706939a.

[14] K. Tomoda, H. Terashima, K. Suzuki, T. Inagi, H. Terada, K. Makino, Enhanced transdermal delivery of indomethacin-loaded PLGA nanoparticles by iontophoresis, Colloids Surfaces B Biointerfaces. 88 (2011) 706–710. doi:10.1016/j.colsurfb.2011.08.004.

[15] Daniel S.Straus, Effects of insulin on cellular growth and proliferation, Life Sci. 29 2131-2139. 29 (1981) 2131–39. doi:https://doi.org/10.1016/0024-3205(81)90482-3.

[16] S.Sd. TRiley, TGovender, SStolnik, C.DXiong, M.CGarnett, LIllum, Colloidal stability and drug incorporation aspects of micellar-like PLA-PEG nanoparticles, Colloids Surfaces B Biointerfaces. 16 (1999) 147–159. doi:https://doi.org/10.1016/S0927-7765(99)00066-1.

[17] G.-H. Chun-LiangLo, Meng-HanChou, Pei-LinLu, I-WenLo, Yi-TingChiang, Shang-YuHung, Chieh-YuYang, Shuian-YinLin, Shiaw-PyngWey, Jem-MauLo, The effect of PEG-5K grafting level and particle size on tumor accumulation and cellular uptake, Int. J. Pharm. 456 (2013) 424–431. doi:https://doi.org/10.1016/j.ijpharm.2013.08.045.

[18] P. Boukamp, Normal Keratinization in a Spontaneously Immortalized, Jcb.rupress.org. 106 (1988) 761–771.

[19] D.H. Abdelkader, S.A. El-Gizawy, A.M. Faheem, P.A. McCarron, M.A. Osman, Effect of process variables on formulation, in-vitro characterisation and subcutaneous delivery of insulin PLGA nanoparticles: An optimisation study, J. Drug Deliv. Sci. Technol. 43 (2018) 160–171. doi:10.1016/j.jddst.2017.10.004.

[20] T. Feczkó, J. Tóth, G. Dósa, J. Gyenis, Optimization of protein encapsulation in PLGA nanoparticles, Chem. Eng. Process. Process Intensif. 50 (2011) 757–765. doi:10.1016/j.cep.2011.06.008.

[21] W. Abdelwahed, G. Degobert, S. Stainmesse, H. Fessi, Freeze-drying of nanoparticles: Formulation, process and storage considerations☆, Adv. Drug Deliv. Rev. 58 (2006) 1688–1713. doi:10.1016/j.addr.2006.09.017.

[22] M.H. Mj, K. Ah, M. Mohd, A. Mmr, S. Liza, S. Mj, T.J. Be, a Simple and Sensitive Hplc Method for the Determination of Insulin in Rat Plasma and Its Application in Pharmacokinetic Study, Int. J. Pharm. Pharm. Sci. 5 (2013) 1–5.

[23] S. Papadimitriou, D. Bikiaris, Novel self-assembled core–shell nanoparticles based on crystalline amorphous moieties of aliphatic copolyesters for efficient controlled drug release, J. Control. Release. 138 (2009) 177–184. doi:10.1016/j.jconrel.2009.05.013.

[24] M. García-Díaz, C. Foged, H.M. Nielsen, Improved insulin loading in poly(lactic-co-glycolic) acid (PLGA) nanoparticles upon self-assembly with lipids, Int. J. Pharm. 482 (2015) 84–91. doi:10.1016/j.ijpharm.2014.11.047.

[25] J. Liu, S.M. Zhang, P.P. Chen, L. Cheng, W. Zhou, W.X. Tang, Z.W. Chen, C.M. Ke, Controlled release of insulin from PLGA nanoparticles embedded within PVA hydrogels, J. Mater. Sci. Mater. Med. 18 (2007) 2205–2210. doi:10.1007/s10856-007-3010-0.

[26] M. Hrynyk, M. Martins-Green, A.E. Barron, R.J. Neufeld, Sustained prolonged topical delivery of bioactive human insulin for potential treatment of cutaneous wounds, Int. J. Pharm. 398 (2010) 146–154. doi:10.1016/j.ijpharm.2010.07.052.

[27] American Type Culture Collection, MTT Cell Proliferation Assay Instruction Guide, Components. 6597 (2011) 1–6.

[28] E. Macia, M. Ehrlich, R. Massol, E. Boucrot, C. Brunner, T. Kirchhausen, Dynasore, a Cell-Permeable Inhibitor of Dynamin, Dev. Cell. 10 (2006) 839–850. doi:10.1016/j.devcel.2006.04.002.

[29] K. Yin Win, S.-S. Feng, Effects of particle size and surface coating on cellular uptake of polymeric nanoparticles for oral delivery of anticancer drugs, Biomaterials. 26 (2005) 2713–2722. doi:10.1016/j.biomaterials.2004.07.050.

[30] M. Noori Koopaei, M.R. Khoshayand, S.H. Mostafavi, M. Amini, M.R. Khorramizadeh, M. Jeddi Tehrani, F. Atyabi, R. Dinarvand, Docetaxel Loaded PEG-PLGA Nanoparticles: Optimized Drug Loading, In-vitro Cytotoxicity and In-vivo Antitumor Effect., Iran. J. Pharm. Res. IJPR. 13 (2014) 819–33. http://www.pubmedcentral.nih.gov/articlerender.fcgi?artid=4177642&tool=pmcentrez&re

ndertype=abstract.

[31] M.. Hans, A.. Lowman, Biodegradable nanoparticles for drug delivery and targeting, Curr. Opin. Solid State Mater. Sci. 6 (2002) 319–327. doi:10.1016/S1359-0286(02)00117-1.

[32] a. Beletsi, Z. Panagi, K. Avgoustakis, Biodistribution properties of nanoparticles based on mixtures of PLGA with PLGA–PEG diblock copolymers, Int. J. Pharm. 298 (2005) 233–241. doi:10.1016/j.ijpharm.2005.03.024.

[33] E. Sah, H. Sah, Recent Trends in Preparation of Poly (lactide- co -glycolide) Nanoparticles by Mixing Polymeric Organic Solution with Antisolvent, J. Nanomater. 2015 (2015) 1–23.

[34] B. Zanetti-Ramos, M. Soldi, V. Soldi, E. Lemos-Senna, The effect of polyethylene glycol on drug content, particle morphology, and carbamazepine release profiles of sustained release microspheres prepared from cellulose acetate butyrate, Acta Farm. Bonaer. 25 (2006) 177–183.

[35] F. Danhier, E. Ansorena, J.M. Silva, R. Coco, A. Le Breton, V. Préat, PLGA-based nanoparticles: An overview of biomedical applications, J. Control. Release. 161 (2012) 505–522. doi:10.1016/j.jconrel.2012.01.043.

[36] B. Mukherjee, K. Santra, G. Pattnaik, S. Ghosh, Preparation, characterization and in-vitro evaluation of sustained release protein-loaded nanoparticles based on biodegradable polymers., Int. J. Nanomedicine. 3 (2008) 487–96. doi:10.2147/IJN.S3938.

[37] C. Liang, A.Y. Park, J. Guan, In vitro scratch assay : a convenient and inexpensive method for analysis of cell migration in vitro, Nat. Protoc. 2 (2007) 329–333. doi:10.1038/nprot.2007.30.

[38] M. Fronza, B. Heinzmann, M. Hamburger, S. Laufer, I. Merfort, Determination of the wound healing effect of Calendula extracts using the scratch assay with 3T3 fibroblasts, Ethnopharmacology. 126 (2009) 463–467. doi:10.1016/j.jep.2009.09.014.

[39] Y. Hu, J. Xie, Y.W. Tong, C.-H. Wang, Effect of PEG conformation and particle size on the cellular uptake efficiency of nanoparticles with the HepG2 cells., J. Control. Release. 118 (2007) 7–17. doi:10.1016/j.jconrel.2006.11.028.

[40] B.K. Talupula, Cytotoxicity of PBN spin trap on A204 cells, J. Adv. Pharm. Res. 2 (2011) 9–17.

[41] L. Treuel, X. Jiang, G.U. Nienhaus, New views on cellular uptake and trafficking of manufactured nanoparticles New views on cellular uptake and trafficking of manufactured nanoparticles, J R Soc Interface. 10: 201209 (2013) 1–14.

[42] T. Wang, J. Bai, X. Jiang, G.U. Nienhaus, Cellular uptake of nanoparticles by membrane penetration: A study combining confocal microscopy with FTIR spectroelectrochemistry, ACS Nano. 6 (2012) 1251–1259. doi:10.1021/nn203892h.

[43] C.-L. Chen, W.-H. Hou, I.-H. Liu, G. Hsiao, S.S. Huang, J.S. Huang, Inhibitors of clathrin-dependent endocytosis enhance TGFbeta signaling and responses., J. Cell Sci. 122 (2009) 1863–1871. doi:10.1242/jcs.038729.

[44] J. Chen, S. Li, Q. Shen, H. He, Y. Zhang, Enhanced cellular uptake of folic acid-conjugated PLGA-PEG nanoparticles loaded with vincristine sulfate in human breast cancer, Drug Dev. Ind. Pharm. 37 (2011) 1339–1346. doi:10.3109/03639045.2011.575162.